Crew Dragon: On-Orbit Operations

A Simultation of SpaceX's Crew Dragon and the mission of Rendezvous & Docking with the International Space Station

Christopher Covert

AA 279D - Spacecraft Formation-Flying and Rendezvous
Stanford University

Revision History

Table 1: Project Changelog

Rev	Changes
PS1	- Created document - Added PS1 material
PS2	- Implemented PS1 changes - Added PS2 material - Added List of Figures
PS3	- Implemented PS2 changes - Added error plots - Added PS3 material

Contents

List of Figures

1 Abstract

This report outlines a detailed formation-flying and rendezvous simulation which summarizes the following fundamental Guidance, Navigation, and Control (GNC) requirements: Keplerian orbital mechanics and orbital perturbations; the general relative motion problem; linear formation-flying dynamics and control; impulsive station-keeping and reconfiguration; high-order relative motion equations; formulation of relative motion using orbital elements; perturbation-invariant formations; nonlinear formation control; low-thrust propulsion for formation flying; relative navigation using GNSS and optical navigation.

The generation of this report is supported in part by SpaceX's Paul Forquera (Director of GNC) and Justin Smith (Manager of Dragon GNC) to coincide with an Associate Engineering position to take place during the Summer of 2018 under the supervision of Dragon 2 GNC managers for the purpose of on-orbit operations with the International Space Station (ISS).

2 Mission Proposals

The following mission proposals represent two of SpaceX's leading satellite-based high-profile missions. Due to the lack of publicly available information on Crew Dragon mission specifications, analogies will be drawn from Dragon CRS-14 whenever possible to provide an accurate estimate of orbit planning based upon mission objectives and absolute/relative orbit parameters.

2.1 Primary Candidate: Dragon 2

The following information is taken from the launch of Dragon CRS-14 with the accompanying TLE in Appendix A:

- Mission Name and Operator
  - SpaceX CRS-14, USA
  - Contracted: NASA, Flown: SpaceX
- Mission Objectives
  - Scientific Investigations Cargo
    - RemoveDebris Satellite:a small satellite mission by Surrey NanoSatellite Technology Ltd. under a European Union Framework 7 research project to develop and fly a low-cost demonstrator for the key aspects of Active Debris Removal missions on a quest to address the growing space debris problem. The 100-Kilogram, cube-shaped satellite - the largest deployed from the International Space Station to date (2018) - will demonstrate active debris removal techniques by releasing, tracking and capturing two small CubeSats called DebrisSATs, in the process demonstrating different rendezvous, capture and deorbiting techniques to evaluate their feasibility for operational debris removal missions of the future.
    - MISSE Flight Facility:The Materials on ISS Experiment - Flight Facility (MISSE-FF) builds on the success of the original MISSE Passive Experiment Container concept which consisted of smaller and larger sample plates containing a variety of surface materials for exposure to the space environment outside the International Space Station for varying durations to inform

satellite designers on how different materials degrade over time. The MISSE-FF project created a platform capable of holding 14 exchangeable sample modules for powered & heated payloads as well as passive experiments.

- ASIM: the Atmosphere-Space Interactions Monitor, is an ESA science instrument taking up residence outside the Columbus Module of the International Space Station to study Transient Luminous Events (TLEs) in Earth's upper atmosphere like Blue Jets, Red Sprites and Elves via a suite of cameras and photometers sensitive in a broad wavelength range to reveal previously unknown details of the electrical and chemical processes ongoing where the atmosphere and space interact.
- PFCS Spare: The third Trunk Payload riding on the Dragon SpX-14 mission is not a science/utilization instrument like its two companions but a potentially critical spare part for the Space Station's Thermal Control System. The Pump Flow Control Subassembly, PFCS for short, is a critical component of the ISS Photovoltaic Thermal Control System (PVTCS) in that it routes ammonia coolant to transport heat from the various electrical assemblies located within the Integrated Equipment Assembly to a Photovoltaic Radiator where it is dissipated into space.

- Number and Type of Satellites
  - One CRS Dragon C110.2 for ISS Resupply
  - One International Space Station
- Absolute and Relative Orbit Parameters
  - Reference system: Geocentric
  - Regime: Low Earth
  - Launch date: 2 April 2018, 20:30:38 UTC
  - Perigee Altitude: 410.1 km
  - Apogee Altitude: 412.7 km
  - Period: 92.6 minutes
  - More information available in Section 3.1
- Basic Description of Functioning/Scientific Principle
  - The Dragon spacecraft rendezvoused with the ISS April 4th, 2018 in order to complete a scheduled resupply mission. After an r-bar rendezvous maneuver, it was captured by Canadarm2 at 10:40 UTC and was berthed to the Harmony module at 13:00 UTC. It is scheduled to remain there for approximately one month before de-orbiting and returning to Earth [2].
- Key GNC Requirements
  - For the purpose of on-orbit navigation, Dragon has a suite of Inertial Measurement Units (IMU), GPS Systems, Iridium Recovery Beacons, and Star Trackers. Both the IMUs and star trackers have an accuracy of 0.004° or smaller. The threshold of attitude control is also 0.012° on each axis in station-keeping Mode [4]. As a Dragon module, the following GNC requirements are required for successful rendezvous: GNC bay door deploys, exposing the GNC sensor suite; star tracker attitude initiation works as expected; TDRSS S-band telemetry and commanding works

as expected; demonstrates precision R-bar arrival at 350 m below the ISS; initializes proximity sensors (LIDARs and thermal imagers) and converges a solution for range and range rate before proceeding; demonstrates hold and retreats commanded by the ISS crew; enters free drift at 10 m from the ISS with minimal vehicle body rates; successfully berths to Node 2 Nadir[6].

- Classification
  - Nadir Berthing Rendezvous

2.2 Secondary Candidate: Starlink Constellation

The following information is taken from the launch of Tintin A & B with the accompanying TLEs in Appendix A:

- Mission Name and Operator
  - SpaceX Starlink, USA
- Mission Objectives
  - Develop a low-cost, high-performance satellite bus and requisite customer ground transceivers to implement a new space-based Internet communication system. Secondary objectives include the sale of satellites that use the same satellite bus that may be used for scientific or exploratory purposes in order to fund future Mars transport projects. [7]
- Number and Type of Satellites
  - Two Smallsat-class communication satellites Tintin A & B
- Absolute and Relative Orbit Parameters
  - Both:
    - Reference system: Geocentric
    - Regime: Low Earth
    - Orbit Type: Sun-Synchronous
    - Launch date: 22 February 2018
  - Tintin A
    - Perigee Altitude: 504.2 km
    - Apogee Altitude: 526.5 km
    - Period: 94.8 minutes
    - Epoch: 15 April 2018, 15:18:56 UTC.
    - $a = 6886.14$ km
    - $e = 0.0016$
    - $i = 97.4630°$
    - $\Omega = 114.1702°$

- $\omega = 97.6203°$
- $M_0 = 262.6859°$

– Tintin B

- Perigee: 504.1 km
- Apogee: 526.2 km
- Period: 94.8 minutes
- Epoch: 15 April 2018, 5:12:45 UTC.
- $a = 6886.35$ km
- $e = 0.0016$
- $i = 97.4562°$
- $\Omega = 114.6986°$
- $\omega = 91.5260°$
- $M_0 = 268.7829°$

• Basic Description of Functioning/Scientific Principle

– The satellites will employ optical inter-satellite links and phased array beam forming and digital processing technologies in the Ku- and Ka band. Ka- and Ku-band satellites will orbit at an altitude of 1,200 km (750 miles), and V-band satellites will orbit lower at 210 miles (340 km.). The proposed Starlink constellation includes 4,425 higher orbit satellites and 7,518 lower orbit satellites using a peer-to-peer protocol simpler than IPv6. Since each satellite would orbit at 1/30 of geostationary orbits, they offer practical latencies around 25 to 35 ms, comparable to currently existing cable or fiber networks [8].

• Key GNC Requirements

– Not much is known about the Tintin A & B satellites or the Starlink Constellation project due to the nature of these demonstrations as technical proofs of concept in a market that is growing to be increasingly more competitive. Therefore, information regarding the GNC of these satellites is not publicly available.

• Classification

– Communication Satellite Constellation

3 Orbit Simulation

The following orbit simulation and data analysis was conducted on Dragon CRS-14 for a berthing maneuver to the ISS. Whereas Crew Dragon will forgo berthing for a docking approach, CRS-14 provides an accurate measure of orbit parameters that Crew Dragon will be designed to emulate. All initial conditions were derived from the TLE in Appendix A.

3.1 Keplerian Initial Conditions

The initial conditions of the simulation are provided as a set of Keplerian orbital elements and an initial epoch date and time. Since a TLE for this mission is available, initial launch time is replaced with an active epoch time.

Therefore, although the mission has a launch date of 2 April 2018, 20:30:38 UTC, all initial conditions are taken from the TLE at Epoch: 15 April 2018, 12:27:43 UTC.

$a = 6782.42$ km
$e = 0.0002.42$
$i = 51.6438°$
$\Omega = 331.1221°$
$\omega = 355.8915°$
$M_0 = 76.9789°$

3.2 Inertial Position and Velocity Initial Conditions

By treating these initial Keplerian elements as osculating quantities, computing the corresponding initial position and velocity in the appropriate inertial frame (Earth- Centered Inertial for an Earth-orbiting mission), leads to the following vectors:

${r_0}^{ECI} = [\,3689.667,\ 2558.674,\ 5082.996\,]'$ [km]
${v_0}^{ECI} = [\,-5.739,\ 4.764,\ 1.769\,]'$ [km/s]

3.3 Unperturbed Orbit Propagation

For an unperturbed system, vehicle dynamics follow a simple second-order non-linear ODE with zero disturbance forces present. This ODE represents the gravitational acceleration felt on the vehicle in ideal conditions (homogeneous spherical Earth mass model with M_1 ¿¿ M_2 and no external forces). Using the initial inertial states as provided in section 3.2, the following equation can be numerically integrated [1]:

$$\ddot{\mathbf{r}} + \frac{\mu \mathbf{r}}{r^3} = \mathbf{0}$$

By neglecting any perturbations beyond the two-body spherical gravity force acting on the orbit, the following orbit path was produced over a span of 100 complete orbits with a numerical integration step size of 1 second.

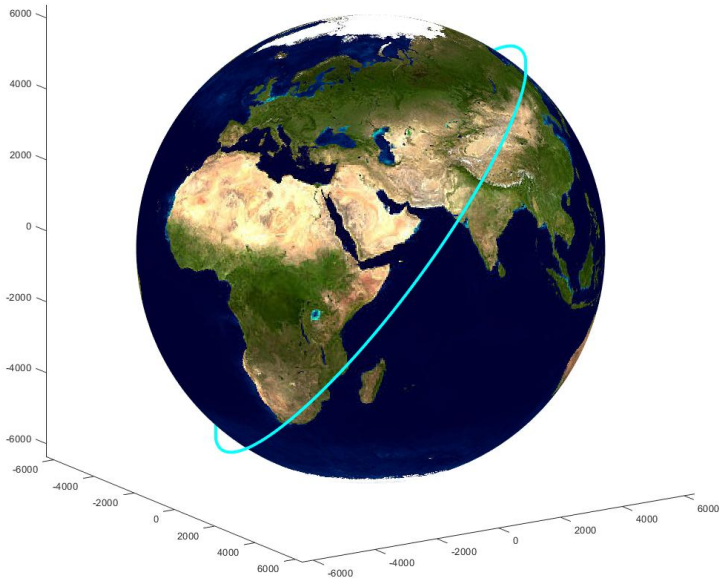

Figure 1: Unperturbed Orbit Path

3.4 Orbit Propagation with J_2 Effects

By considering J_2 effects from Earth oblateness, small disturbances can be introduced into the numerical integration to produce a non-constant orbit path. The governing dynamics then introduce non-zero forces proportional to J_2 as prescribed below [1]:

$$\ddot{X} = -\frac{\mu X}{r^3}\left[1 - \frac{3}{2}J_2\left(\frac{R_e}{r}\right)^2\left(5\frac{Z^2}{r^2} - 1\right)\right]$$
$$\ddot{Y} = -\frac{\mu Y}{r^3}\left[1 - \frac{3}{2}J_2\left(\frac{R_e}{r}\right)^2\left(5\frac{Z^2}{r^2} - 1\right)\right]$$
$$\ddot{Z} = -\frac{\mu Z}{r^3}\left[1 - \frac{3}{2}J_2\left(\frac{R_e}{r}\right)^2\left(5\frac{Z^2}{r^2} - 3\right)\right]$$

The following orbit path was run over the same parameters as Figure 1 with the addition of J_2 effects.

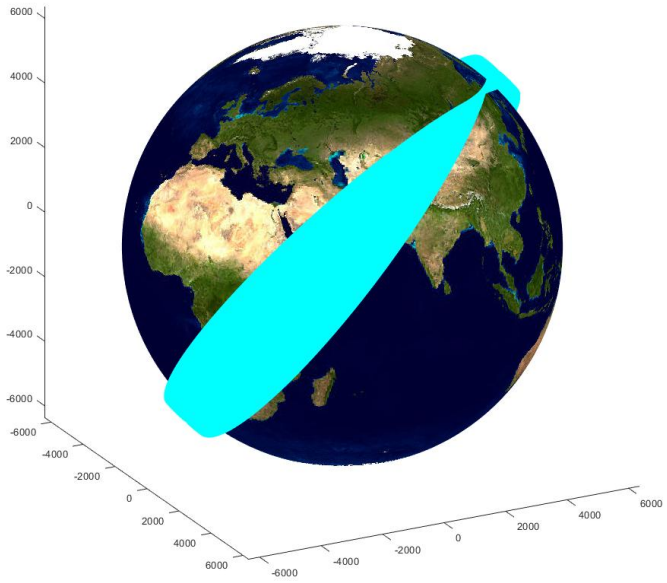

Figure 2: Orbit Path with J_2 Effects

3.5 Error Propagation

By comparing the state output from the unperturbed numerical integration against an analytical Keplerian propagation, the accuracy of the integrator can be demonstrated. The error in absolute position and inertial velocity expressed in the local vertical, local horizontal (RTN) coordinate system can be seen below for a simulation over a span of 10 complete orbits with a numerical integration step size of 1/100,000th of an orbit period.

As the error in the system propagates over the length of the simulation, error accumulated over the span of 10 orbits was shown to accuracy drift and potential divergence.

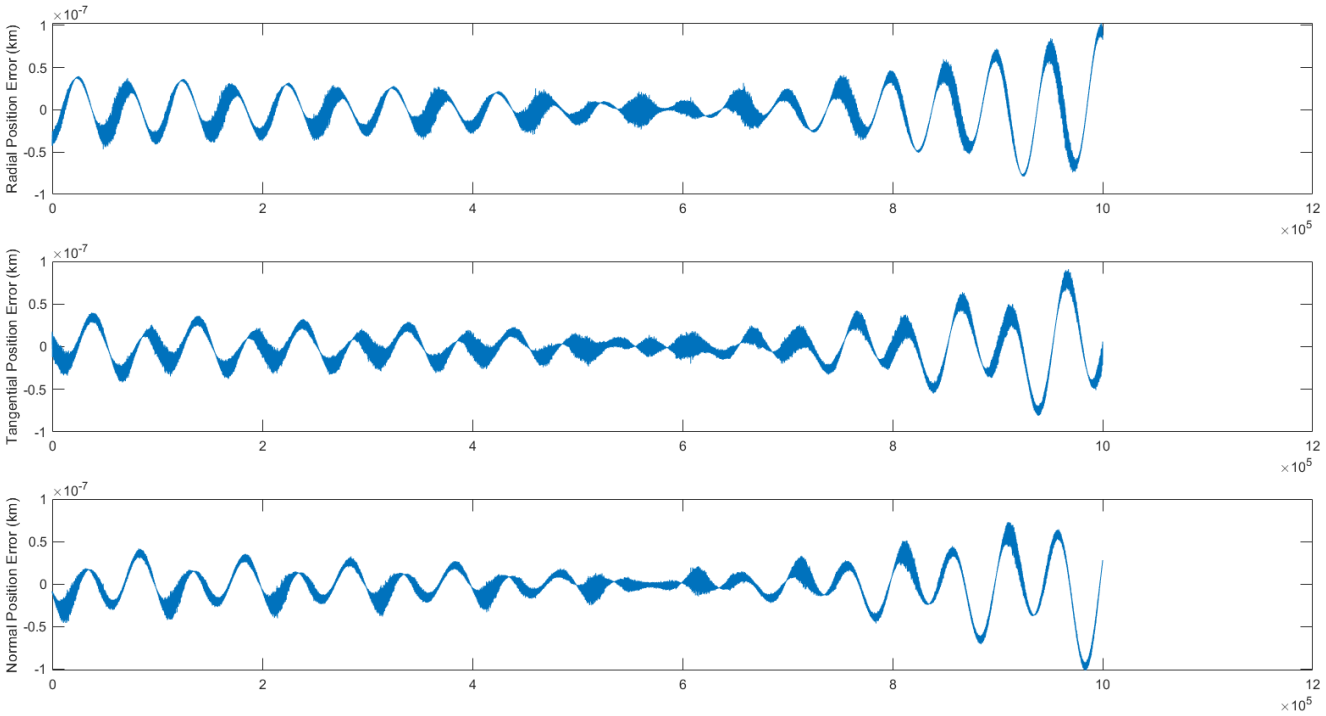

Figure 3: RTN Position Error [km]

As seen in the vertical axis of this plot, the error over 10 orbits is scaled to $10^{-}7$ km, or 0.1 mm. Therefore, the numerically integrated position vector, r^{RTN}, is accurate and has negligible error propagation over 10 orbits.

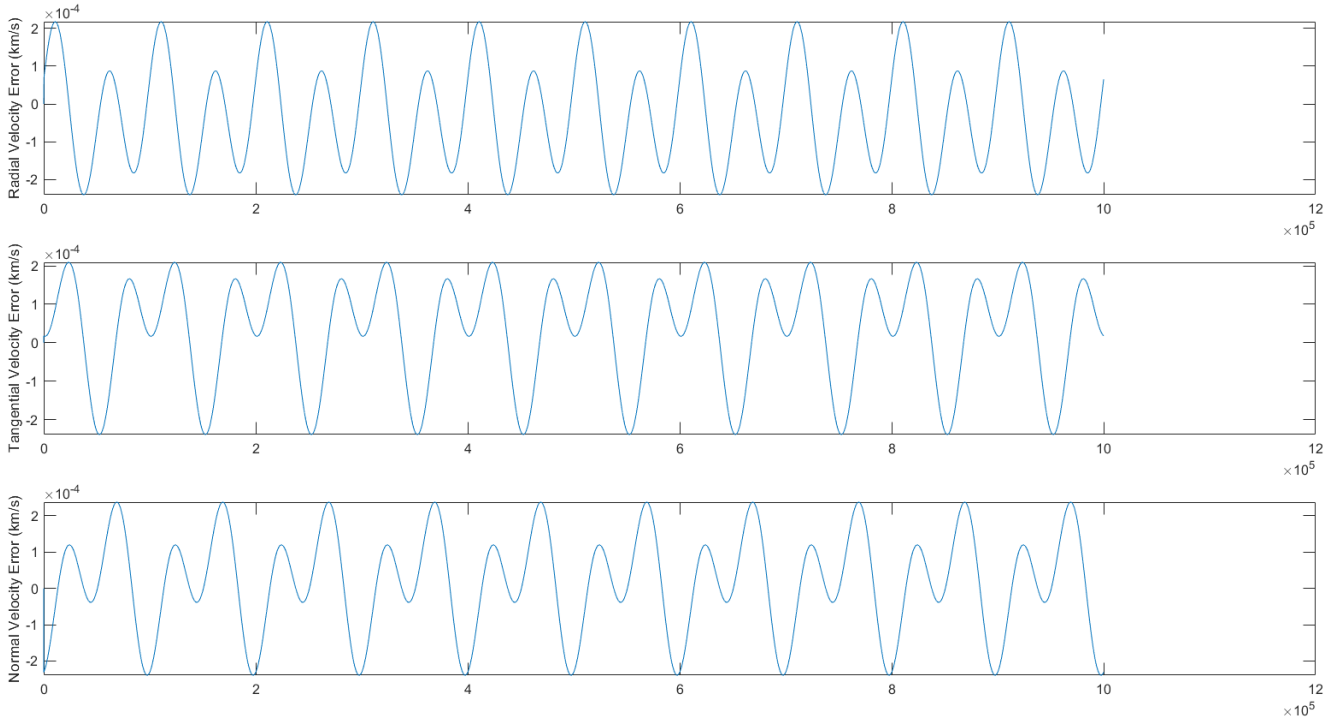

Figure 4: RTN Velocity Error [km/s]

In this plot, the error over 10 orbits is scaled to 10^-4 km, or 1 cm. Therefore, although larger than the positional error, the numerically integrated velocity vector, v^{RTN}, is also accurate and has negligible error propagation over 10 orbits.

3.6 Osculation Disturbances

When excluding J_2 effects, it can be seen that the disturbance-free time history for the Keplerian orbital elements (a, e, i, Ω, ω), the magnitude of the angular momentum, and the specific mechanical energy are all constant. The only non-constant value is the true anomaly, which is monotonically increasing (modulo 360°).

The following was run over a span of 10 complete orbits with a numerical integration step size of 1 second.

With the addition of J_2 effects, the oblateness of the Earth provides a small disturbance in the gravitational acceleration of the vehicle that is no longer constant, but has a low frequency mode relating to its orbit and relative position to the equator.

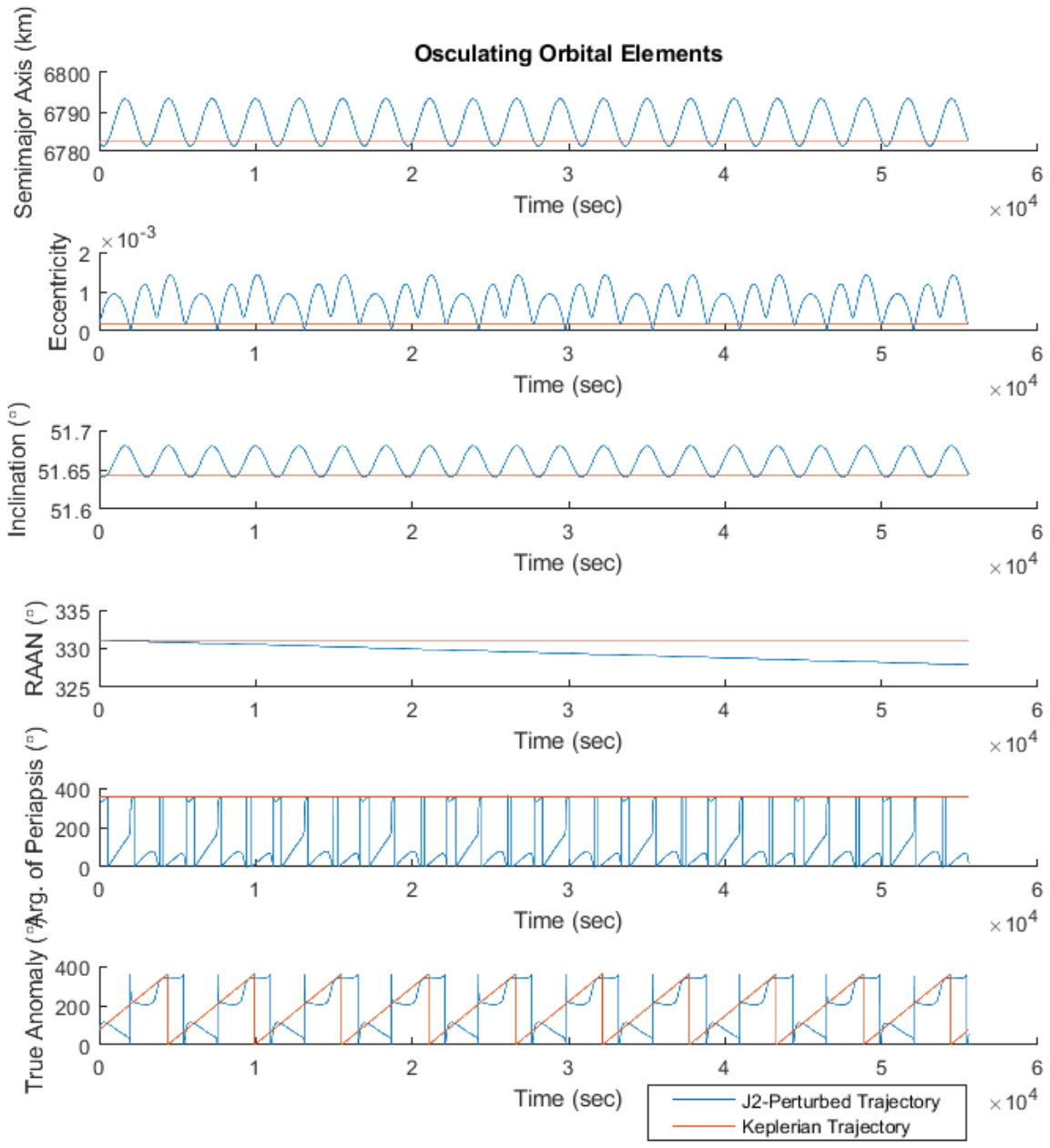

Figure 5: J_2-Affected Osculating Time Histories

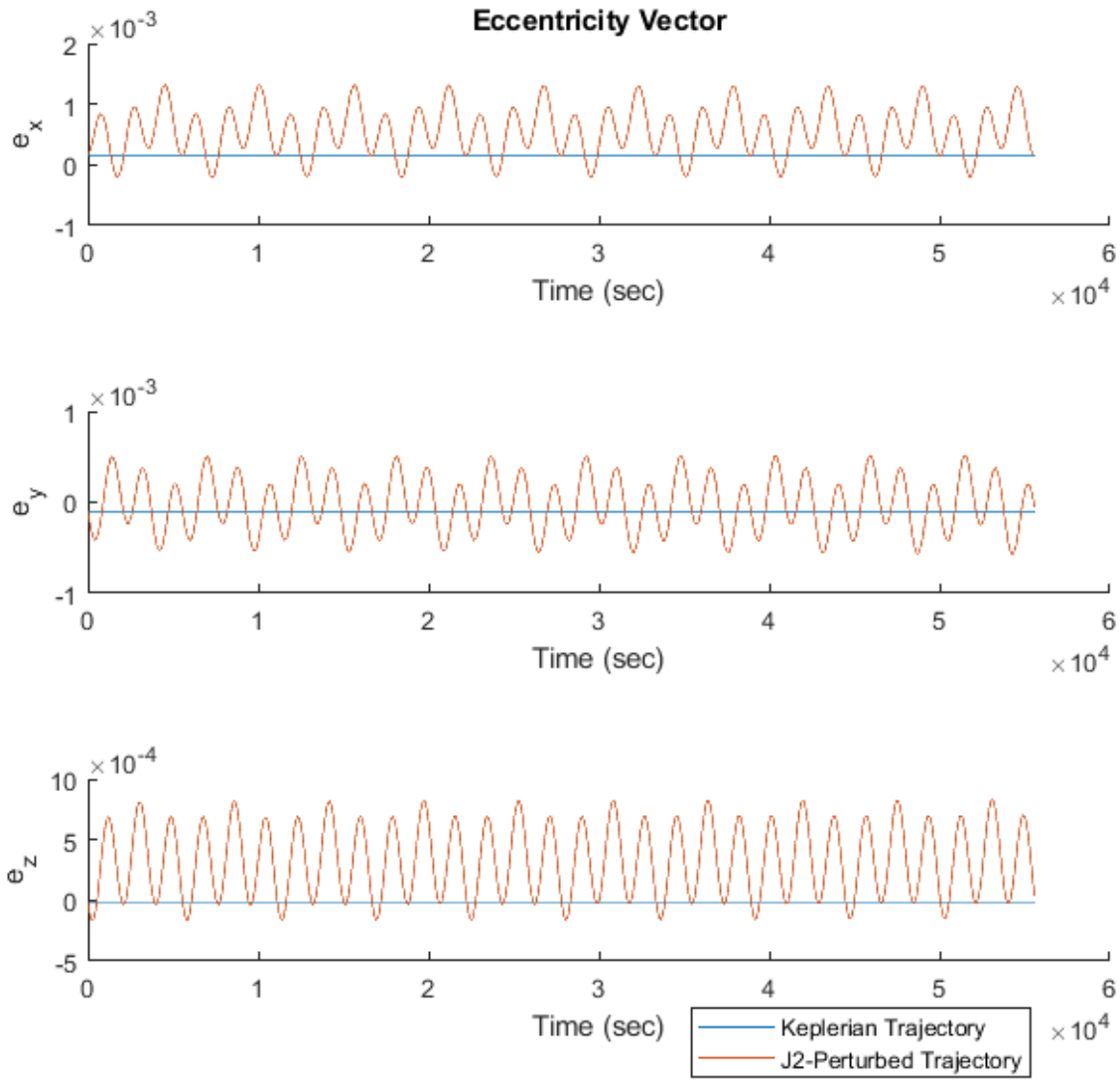

Figure 6: J_2-Affected Osculating Time Histories

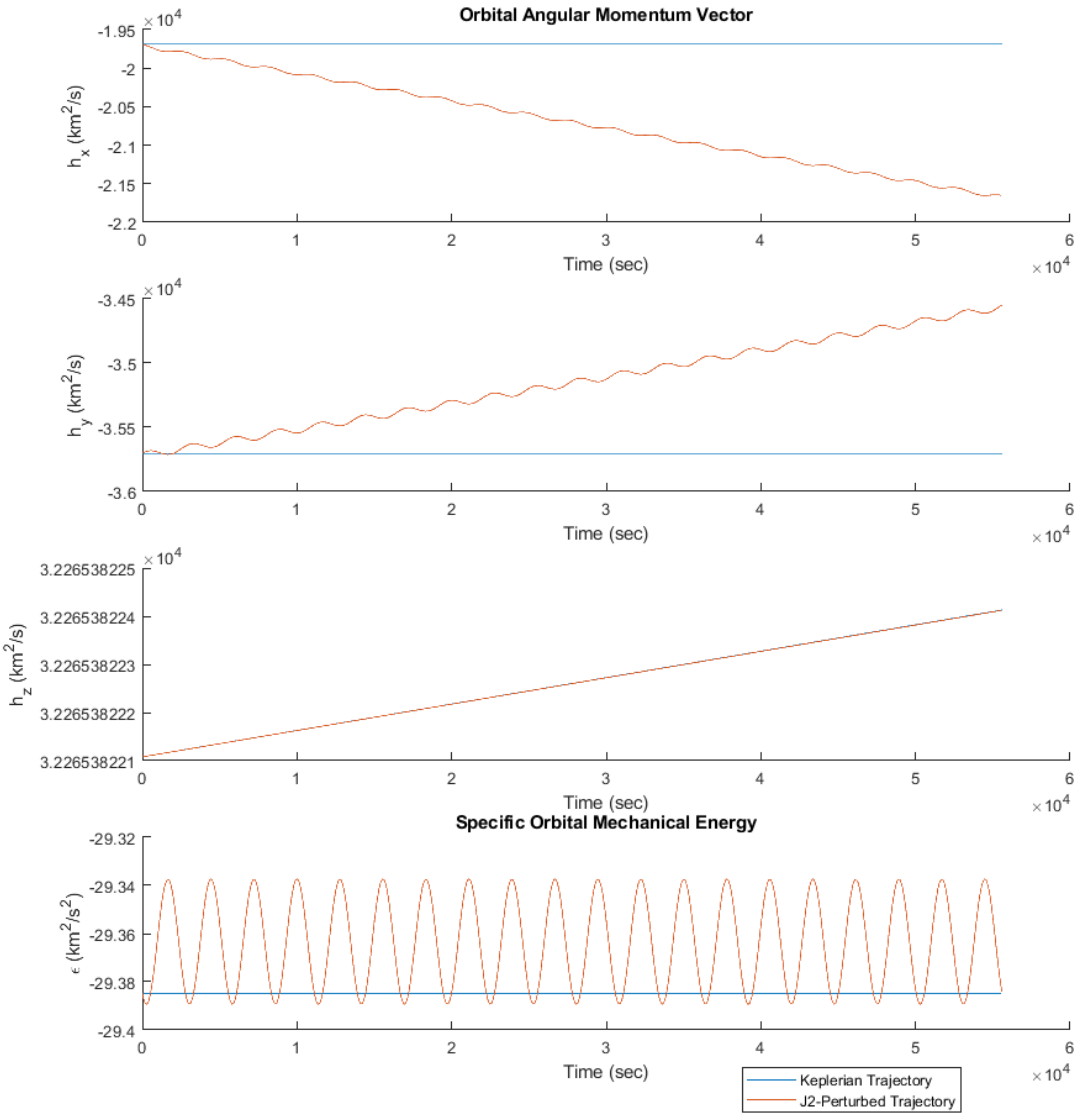

Figure 7: J_2-Affected Osculating Time Histories

Although difficult to see on such a timescale, these results are as expected from the results of averaging theory (discussed in the following section), where the semimajor axis, eccentricity, and inclination only experience periodic changes, while the RAAN, argument of periapsis, and true anomaly undergo both periodic and secular effects.

3.7 Mean Keplerian Orbital Elements

By using Averaging Theory as a comparison to the osculating orbital elements from Figure 6, the following simplified first-order linear ODE's can be used to propagate the mean Keplerian orbital elements with J2 effects [1]:

$$
\begin{aligned}
\frac{\mathrm{d}\bar{a}}{\mathrm{d}t} &= 0 \\
\frac{\mathrm{d}\bar{e}}{\mathrm{d}t} &= 0 \\
\frac{\mathrm{d}\bar{i}}{\mathrm{d}t} &= 0 \\
\frac{\mathrm{d}\bar{\Omega}}{\mathrm{d}t} &= -\frac{3}{2} J_2 \left(\frac{R_e}{\bar{p}} \right)^2 \bar{n} \cos \bar{i} \\
\frac{\mathrm{d}\bar{\omega}}{\mathrm{d}t} &= \frac{3}{4} J_2 \left(\frac{R_e}{\bar{p}} \right)^2 \bar{n} (5 \cos^2 \bar{i} - 1) \\
\frac{\mathrm{d}\bar{M}_0}{\mathrm{d}t} &= \frac{3}{4} J_2 \left(\frac{R_e}{\bar{p}} \right)^2 \bar{n} \bar{\eta} (3 \cos^2 \bar{i} - 1)
\end{aligned}
$$

It should be noted that the inputs for this system are mean elements, not instantaneous ones. The following plot compares the osculating orbital elements (solid, red) to the expected mean Keplerian orbital elements with J_2 effects (dotted, black).

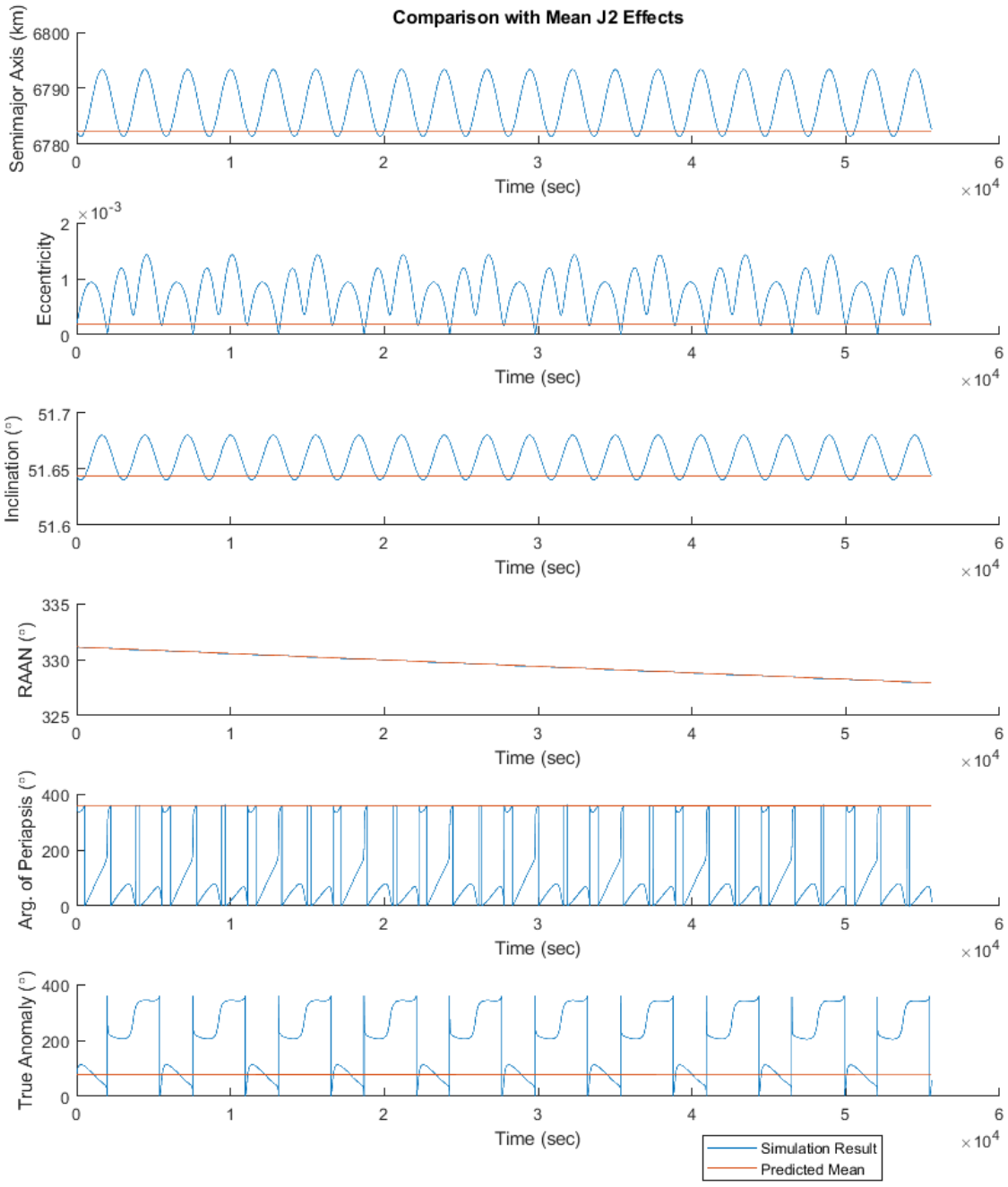

Figure 8: Mean and Osculating Keplerian Orbital Elements

Clearly, the mean orbital elements represent the mean of the osculating orbital elements as expected from Averaging Theory.

3.8 Inconsistencies in Mean vs. Osculating Element Methods

It is possible to encounter inconsistencies when comparing osculating and mean orbital elements due the initialization procedure. In fact, one uses osculating states as inputs and provides osculating states as outputs, whereas the other uses mean states as inputs and provides mean states as outputs.

Since the mean states cannot be calculated without the osculating orbit, it is possible to run a simulation of a single orbit to provide enough information to initialize the mean states. Therefore, if computational costs are a factor, the calculation of the osculating orbital elements must only be computed for one orbit and the mean Keplerian orbital elements may be used for the remainder of the calculation. It should be noted, however, that the stronger the J_2 effects are on the orbit, the greater the standard deviation in the osculating terms from the mean terms (which increasing instantaneous error).

In order to convert between osculating and mean orbital elements, a few methods are available: Brouwer's Satellite Theory, Short-Period Kozai-Izsak theory, and Eckstein-Ustinov theory to name a few (variations on PLEs and GVEs).

4 Relative Motion

4.1 Initial Conditions

The chief orbit in this simulation is taken directly from the initial conditions of the prior simulation in Section 3.1:

Chief:

$a = 6782.42$ km
$e = 0.0002.42$
$i = 51.6438°$
$\Omega = 331.1221°$
$\omega = 355.8915°$
$M_0 = 76.9789°$

From the Chief orbit, small variations were applied to the Keplerian orbital elements to produce a Deputy orbit with a $1°$ change in inclination, Ω, and ω.

Deputy:

$a = 6782.42$ km
$e = 0.0002.42$
$i = 52.6438°$
$\Omega = 332.1221°$
$\omega = 356.8915°$
$M_0 = 76.9789°$

These changes in orbital elements are a valid set of initial conditions due to the relation of relative position to the value of r_0, satisfying:

$$\|\vec{\rho}\| \leq 0.001 \|\vec{r_0}\|$$

4.2 Relative Position and Velocity

A numerical integration of the nonlinear equations of relative motion can be performed on Eqns (4.17) - (4.19) from [1]:

$$\ddot{x} - 2\dot{\theta}_0\dot{y} - \ddot{\theta}_0 y - \dot{\theta}_0^2 x = -\frac{\mu(r_0 + x)}{\left[(r_0 + x)^2 + y^2 + z^2\right]^{\frac{3}{2}}} + \frac{\mu}{r_0^2} + d_x + u_x$$

$$\ddot{y} + 2\dot{\theta}_0\dot{x} + \ddot{\theta}_0 x - \dot{\theta}_0^2 y = -\frac{\mu y}{\left[(r_0 + x)^2 + y^2 + z^2\right]^{\frac{3}{2}}} + d_y + u_y$$

$$\ddot{z} = -\frac{\mu z}{\left[(r_0 + x)^2 + y^2 + z^2\right]^{\frac{3}{2}}} + d_z + u_z$$

From this integration, relative position and velocity vectors can be propagated in the rotating RTN frame with origin at the chief spacecraft.

The following plots were produced over 10 orbits with a step size of 5 seconds.

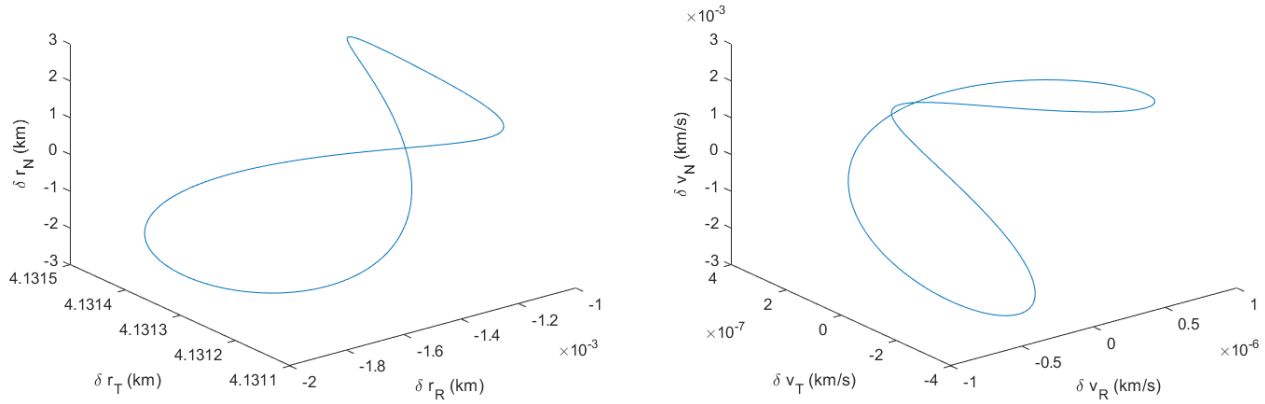

(a) Relative Position (3D)

(b) Relative Velocity (3D)

Figure 9: Relative Position and Velocity in 3D

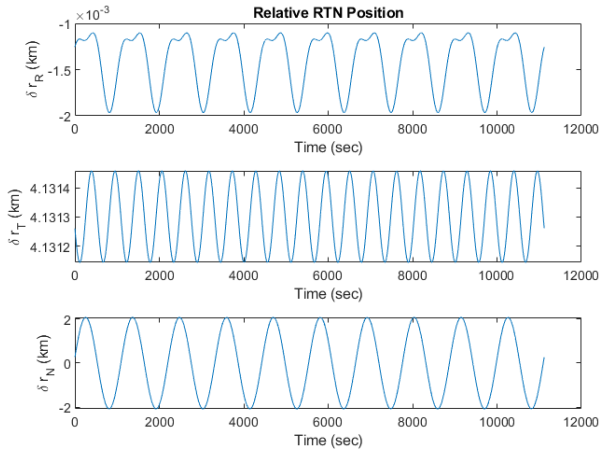

(a) Relative Position

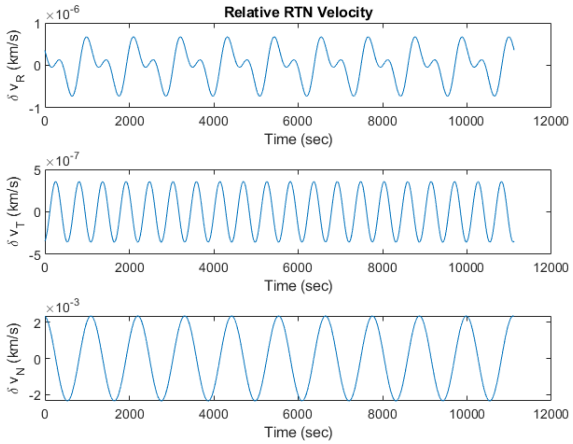

(b) Relative Velocity

Figure 10: Relative RTN Position and Velocity Vectors

4.3 Relative Difference of Absolute Motion

A verification of the numerical integrator can be performed by differencing the results of differential equations of absolute motion for both the chief and deputy orbits.

Below is a plot of the data, showing that both simulations overlap and that the numerical integration of the previous section is held to an order of numerical error, therefore verifying the validity of the integration method.

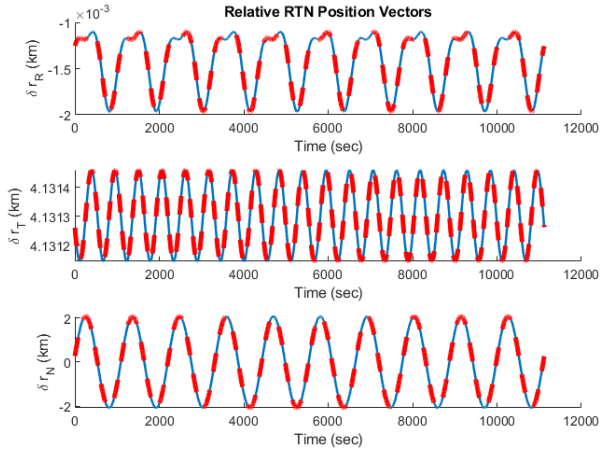

(a) Relative Position Vectors

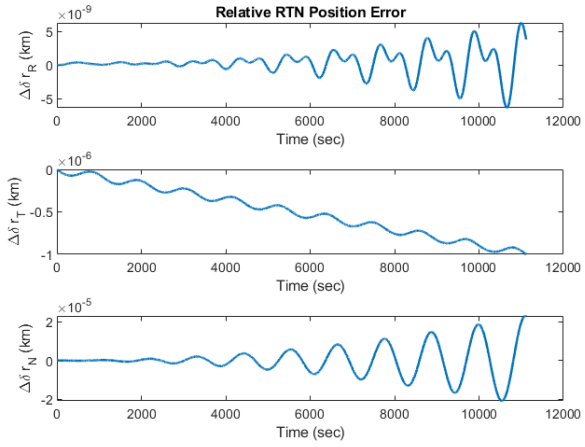

(b) Relative Position Error

Figure 11: Relative RTN Position and Error

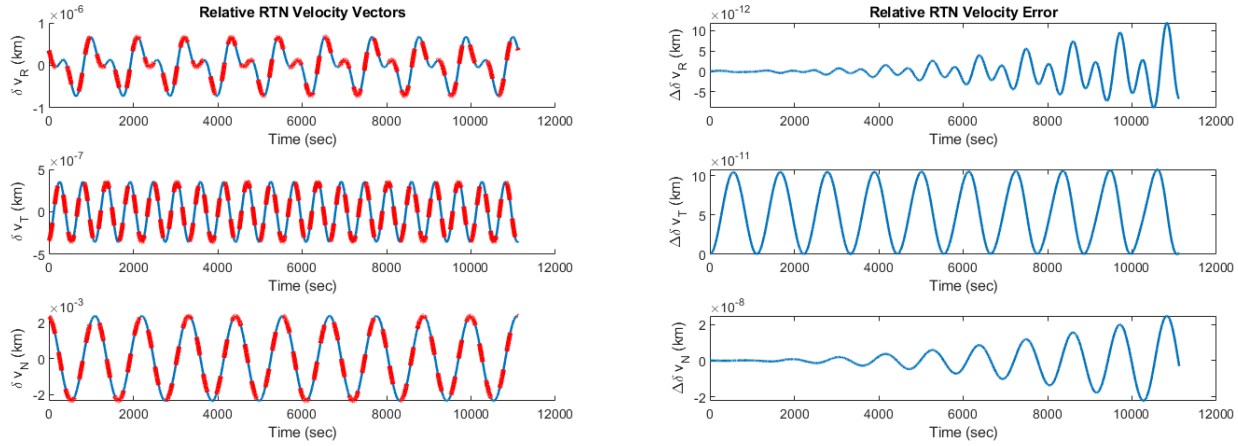

(a) Relative Velocity Vectors (b) Relative Velocity Error

Figure 12: Relative RTN Velocity and Error

4.4 Disturbances to Semi-major Axis

By adding a relative disturbance to the semi-major axis, a difference in mechanical energy is induced, thus leading to a locally unbounded relative motion. With a Δa of 2 km, the following unbounded solution is produced.

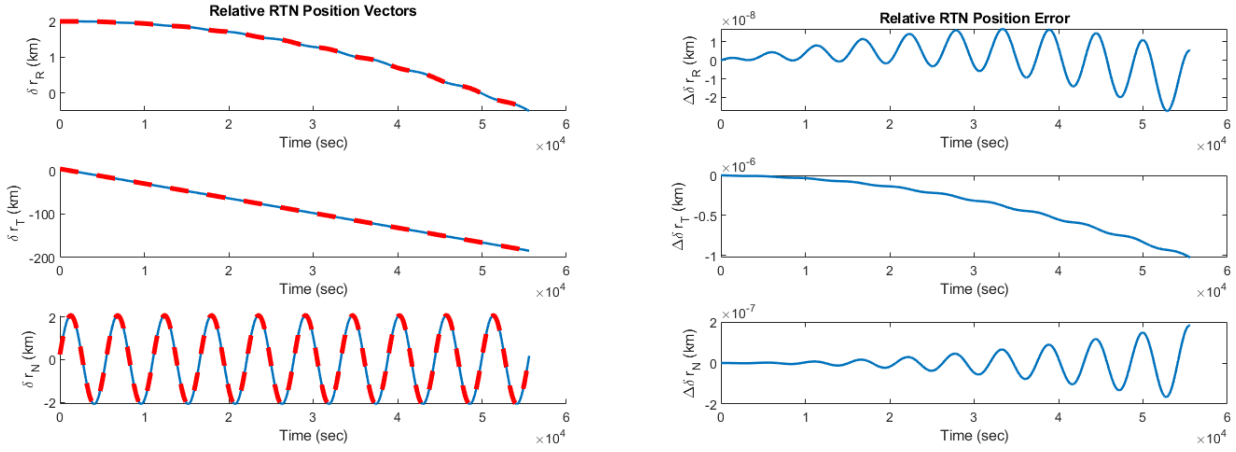

(a) Relative Position Vectors (b) Relative Position Error

Figure 13: Unbounded Relative RTN Position and Error

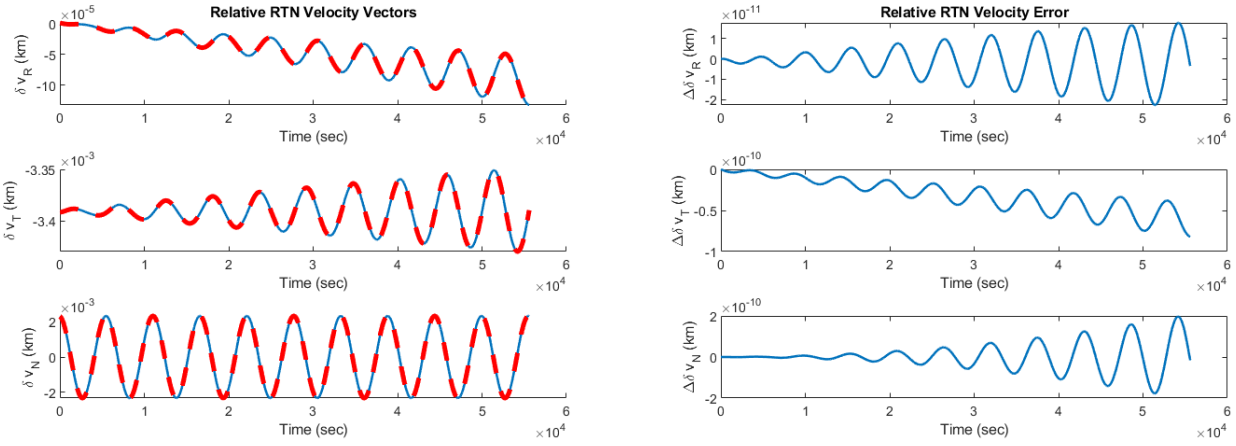

(a) Relative Velocity Vectors (b) Relative Velocity Error

Figure 14: Unbounded Relative RTN Velocity and Error

4.5 Impulsive Formation Keeping

In order to re-establish a bounded periodic relative motion between deputy and chief orbits, the following equations may be used to calculate ΔV:

$$
\begin{aligned}
v_x^- &= \dot{x}^-(t_i) - \dot{\theta}_0^-(t_i)y(t_i) + \dot{r_0}^-(t_i) \\
v_y^- &= \dot{y}^-(t_i) + \dot{\theta}_0^-(t_i)[x(t_i) + r_0(t_i)] \\
v_z^- &= \dot{z}^-(t_i) \\
r_1 &= \sqrt{[r_0(t_i) + x(t_i)]^2 + y^2(t_i) + z^2(t_i)}
\end{aligned}
$$

$$
\frac{\Delta v_x^*}{v_x^-} = \frac{\Delta v_y^*}{v_y^-} = \frac{\Delta v_z^*}{v_z^-} = -1 + \frac{1}{v_1^-}\sqrt{\frac{\mu(2a_0 - r_1)}{a_0 r_1}}
$$

$$
\Delta v^* = \sqrt{(\Delta v_x^*)^2 + (\Delta v_y^*)^2 + (\Delta v_z^*)^2} = v_1^- - \sqrt{\frac{\mu(2a_0 - r_1)}{a_0 r_1}}
$$

ΔV Parameters	
ΔV_x	6.833e-07 km/s
ΔV_y	-1.129e-03 km/s
ΔV_z	-3.419e-07 km/s

Table 2: Minimum-Fuel Impulse ΔV Maneuver

4.6 Discontinuous Inertial Velocity Insertion

The maneuver should take place on the the minimum impulse value in order to save fuel for future maneuvers. In the following plot of ΔV_{total} vs Orbit Count, it can be seen where the best position to fire the impulse lies around the fifth orbit:

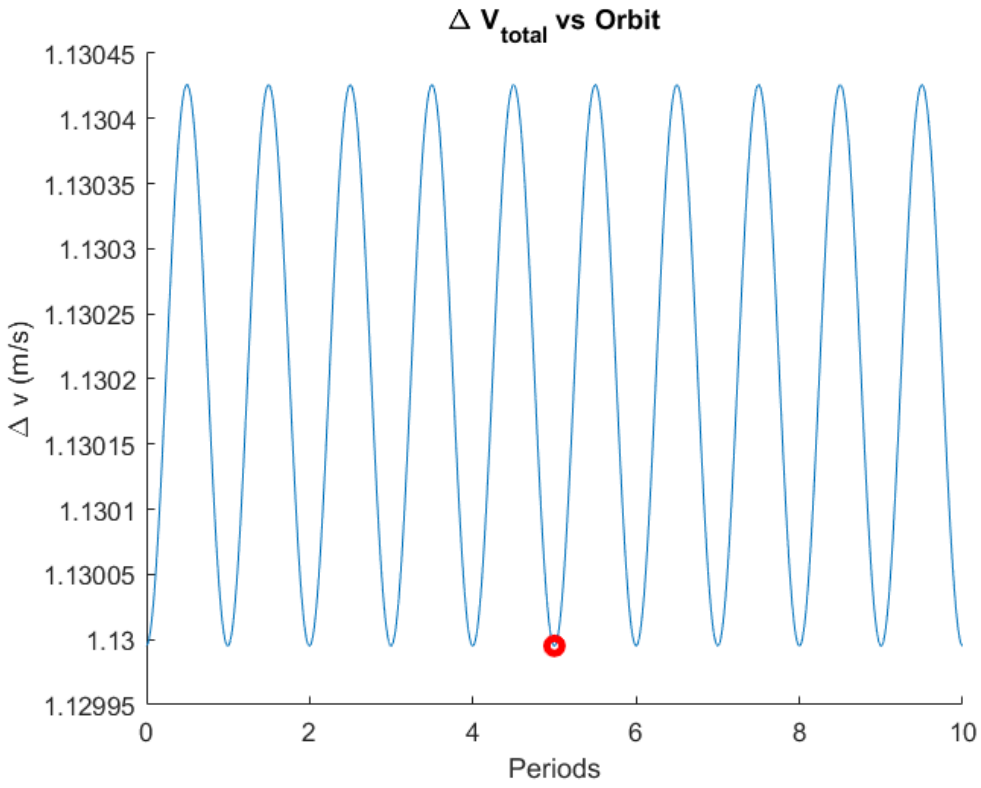

Figure 15: ΔV_{total} vs Orbit Count

From this plot, it can be seen that the first viable location for the impulse is near the initial conditions, but on the fifth orbit. By injecting a discontinuity of ΔV/stepsize as u into the equations of relative motion, a re-establishment of bounded periodic motion may be induced.

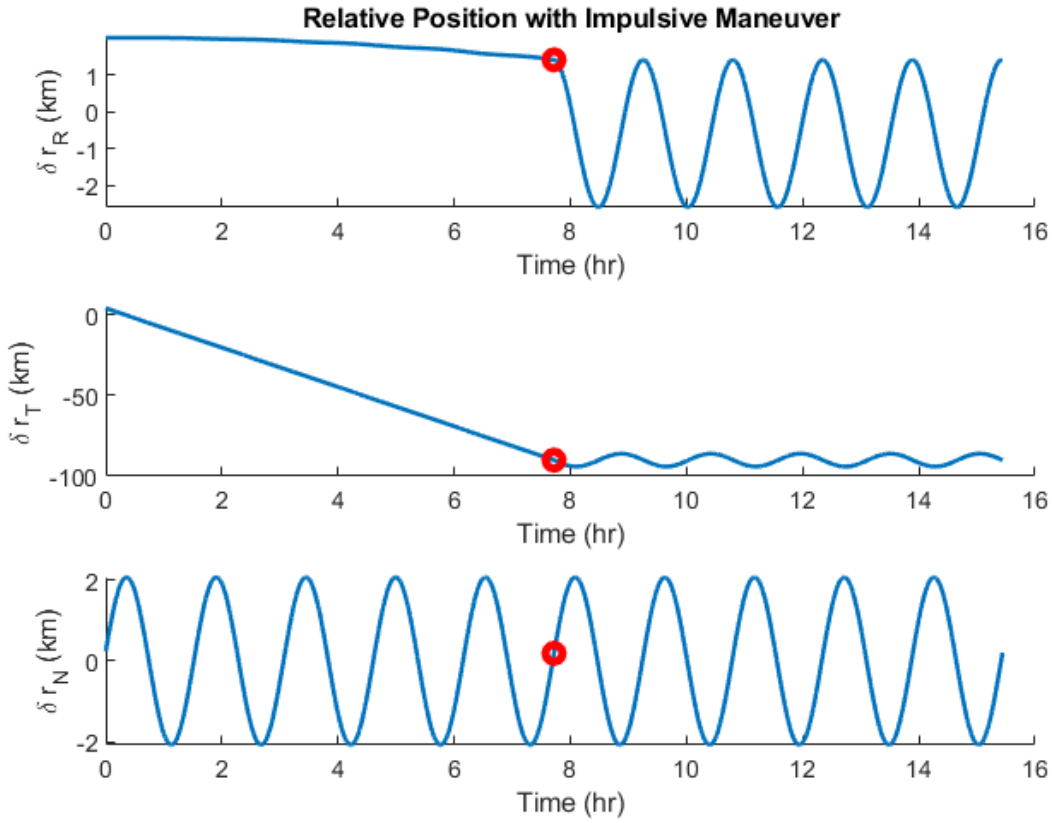

Figure 16: Location of Impulse and Corresponding Relative Position

5 Linear Relative Motion

5.1 Initial Conditions

The initial conditions for this linearized simulation are identical to the conditions used in the previous section.

Chief:

$a = 6782.42$ km
$e = 0.0002.42$
$i = 51.6438°$
$\Omega = 331.1221°$
$\omega = 355.8915°$
$M_0 = 76.9789°$

From the Chief orbit, small variations were applied to the Keplerian orbital elements to produce a Deputy orbit with a 1° change in inclination, Ω, and ω.

Deputy:

$a = 6782.42$ km
$e = 0.0002.42$
$i = 52.6438°$
$\Omega = 332.1221°$
$\omega = 356.8915°$
$M_0 = 76.9789°$

These changes in orbital elements are a valid set of initial conditions due to the relation of relative position to the value of r_0, satisfying:

$$\|\vec{\rho}\| \leq 0.001 \|\vec{r_0}\|$$

By treating these initial Keplerian elements as osculating quantities, computing the corresponding initial position and velocity in the appropriate inertial frame (Earth- Centered Inertial for an Earth-orbiting mission), leads to the following vectors:

Chief:

${r_0}^{ECI} = [\,6730.078,\ 841.009,\ 2.5023\,]'$ [km]
${v_0}^{ECI} = [\,-0.951,\ 7.606,\ 0.121\,]'$ [km/s]

Deputy:

${r_0}^{ECI} = [\,6729.822,\ 843.058,\ 2.5508\,]'$ [km]
${v_0}^{ECI} = [\,-0.953,\ 7.601,\ 0.123\,]'$ [km/s]

From the ECI vectors, relative position and velocity (taken and expressed in the chief RTN frame) can be propagated as such:

Relative Position and Velocity:

${r_0}^{RTN} = [\,-3.146 \cdot 10^{-4},\ 2.066,\ 0.016\,]'$ [km]
${v_0}^{RTN} = [\,-5.388 \cdot 10^{-9},\ -3.557 \cdot 10^{-7},\ 0.002\,]'$ [km/s]

5.2 Rectilinear HCW Propagation

5.2.1 Integration Constants

The analytical solution to the HCW equations can be expressed as follows:

$$x(t) = c_1 + c_2 \sin(nt) + c_3 \cos(nt)$$
$$y(t) = c_4 - 1.5nc_1t + 2c_3 \sin(nt) + 2c_2 \cos(nt)$$
$$z(t) = c_5 \sin(nt) + c_6 \cos(nt)$$

The integration constants of the HCW equations can be expressed from the initial conditions as follows:

$$c_1 = 4x(0) + \frac{2\dot{y}(0)}{n} = -6.2944e-04 \;\; km$$
$$c_2 = \frac{\dot{x}(0)}{n} = -1.0722e-14 \;\; km$$
$$c_3 = -3x(0) - \frac{2\dot{y}(0)}{n} = 6.2944e-04 \;\; km$$
$$c_4 = y(0) - \frac{2\dot{x}(0)}{n} = 2.0658 \;\; km$$
$$c_5 = \frac{\dot{z}(0)}{n} = 2.0662 \;\; km$$
$$c_6 = z(0) = 0.0160 \;\; km$$

5.2.2 Orbit Propagation

Orbit simulation was propagated from a set of differential equations in rectilinear coordinates known as the Hill-Clohessy-Wiltshire (HCW) equations:

$$\ddot{x} - 2n\dot{y} - 3n^2x = 0$$
$$\ddot{y} + 2n\dot{x} = 0$$
$$\ddot{z} + n^2z = 0$$

The following plots were produced with a simulation of 15 orbits and an integration step size of 5 seconds.

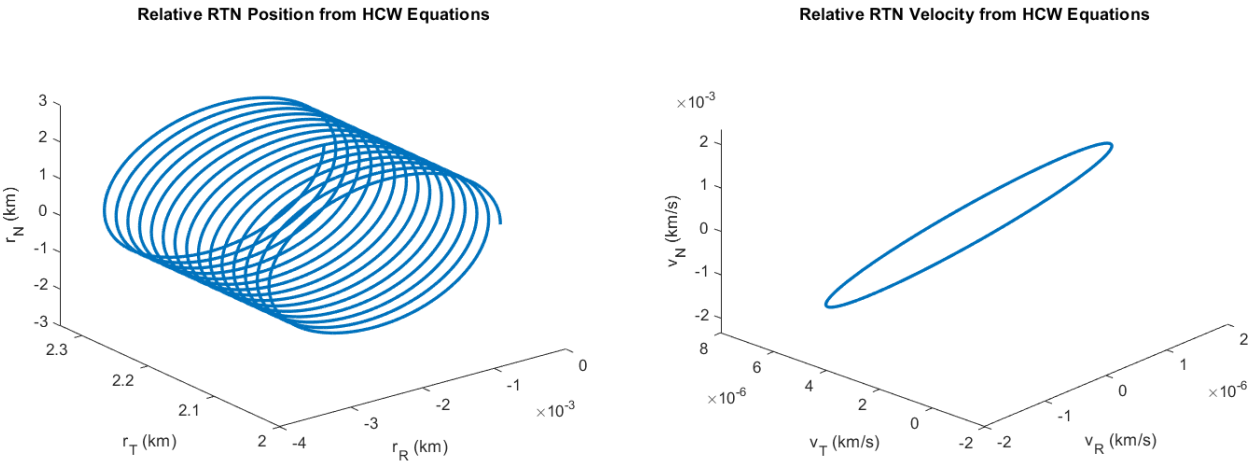

(a) Relative Position (b) Relative Velocity

Figure 17: Relative RTN Position and Velocity Vectors

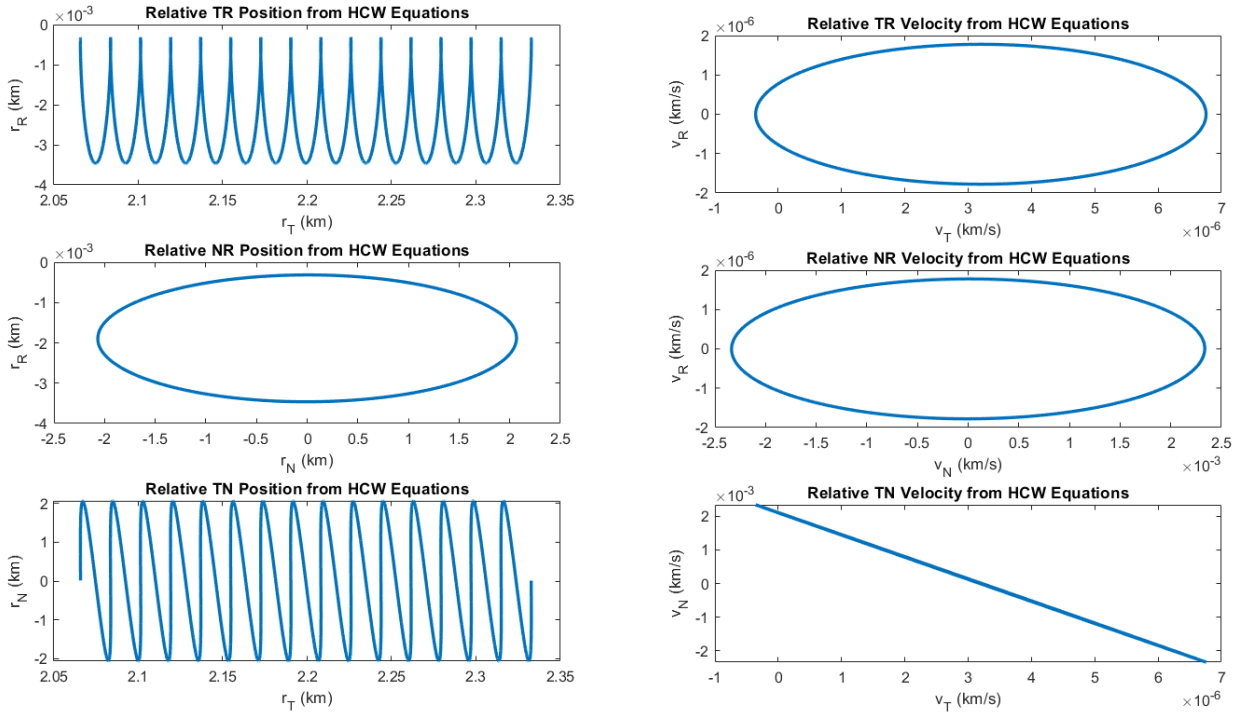

(a) Relative Position

(b) Relative Velocity

Figure 18: Relative RTN Position and Velocity Vectors

This behavior matches the expectation for this orbit to have a drift since the there exist non-zero time-dependent terms in the linearized equations of relative motion. This is also true despite satisfying the energy matching condition since the time dependence no longer bounds periodic motion.

5.3 Curvilinear HCW Propagation

5.3.1 Integration Constants

The HCW equations in curvilinear coordinates have the exact same solution as those for rectilinear coordinates, and so a calculation of the curvilinear integration constants is a simple substitution given by: (x, y, z) $\rightarrow (\delta r, a\theta_r, a\phi_r)$. Now the rectilinear integration constants can be calculated:

$$c_1 = 4\delta r(0) + \frac{2a\dot{\theta}_r(0)}{n} = -0.0019 \;\; km$$

$$c_2 = \frac{\delta\dot{r}(0)}{n} = -4.7675e-06 \;\; km$$

$$c_3 = 3\delta r(0) + \frac{2a\dot{\theta}_r(0)}{n} = 0.0016 \;\; km$$

$$c_4 = a\theta_r(0) - \frac{2\delta\dot{r}(0)}{n} = 2.0658 \;\; km$$

$$c_5 = \frac{a\dot{\phi}_r(0)}{n} = 2.0662 \;\; km$$
$$c_6 = a\phi_r(0) = 0.0160 \;\; km$$

5.3.2 Orbit Propagation

In curvilinear coordinates, the HCW equations take the following form:

$$\delta\ddot{r} - 2a_0 n_0 \dot{\theta}_r - 3n_0^2 \delta r = 0$$
$$a_0\ddot{\theta}_r - 2n_0\delta\dot{r} = 0$$
$$\ddot{\phi}_r + n_0^2\phi_r = 0$$

The following plots were produced with a simulation of 15 orbits and an integration step size of 5 seconds.

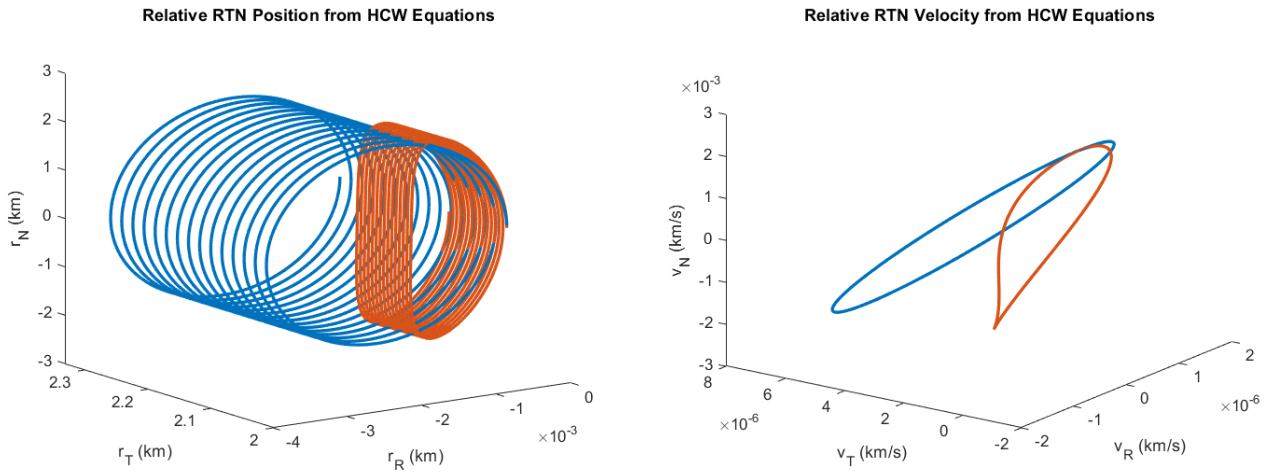

(a) Relative Position (b) Relative Velocity

Figure 19: Relative RTN Position and Velocity Vectors

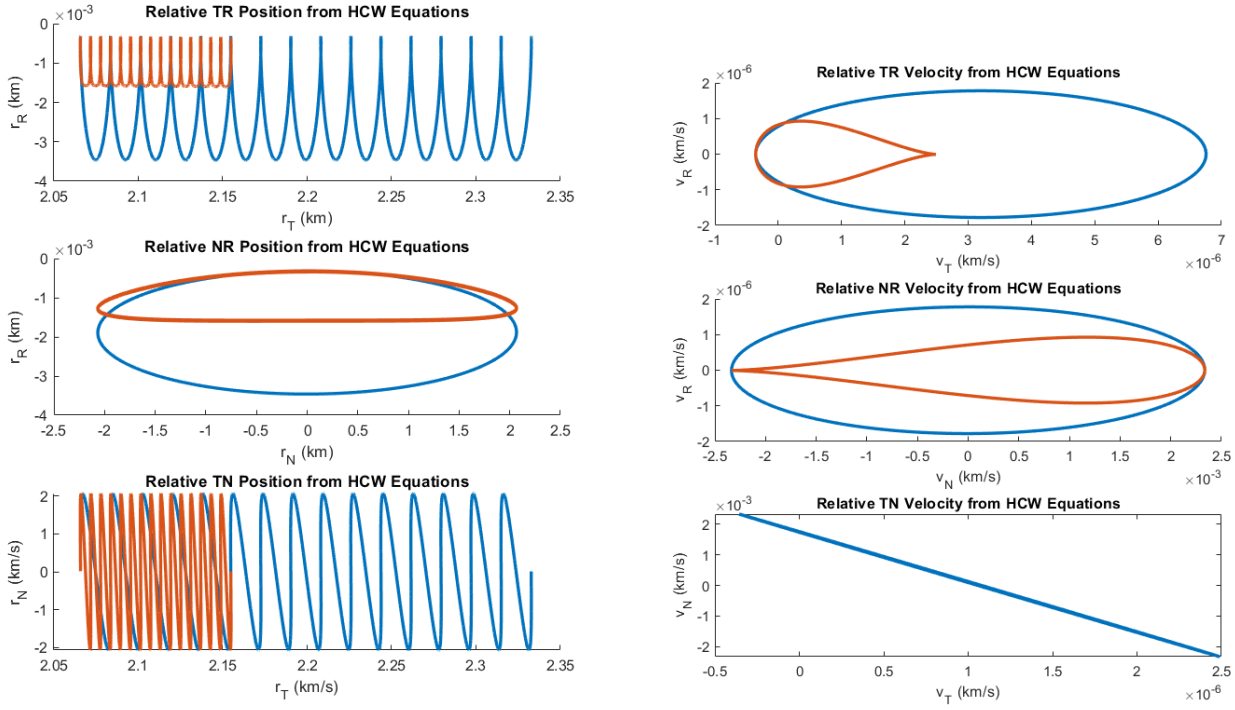

(a) Relative Position

(b) Relative Velocity

Figure 20: Relative RTN Position and Velocity Vectors

A curvilinear transformation on the equations of relative motion relaxes the linearization of the orbit, and reduces the along-track drift error in the linearized propagation. Therefore, we expect the resulting orbit to have a smaller periodic drift as seen in on the superimposed plots.

Appendices

A Two Line Element Sets (TLE)

```
DRAGON CRS14
1 43267U 18032A   18105.51925310 +.00002699 +00000-0 +47756-4 0  9996
2 43267 051.6438 331.1221 0001905 355.8915 076.9789 15.54265438108777

TINTIN A
1 43216U 18020B   18106.53254881  .00002260  00000-0  11029-3 0  9995
2 43216  97.4562 114.6986 0016194  91.5260 268.7829 15.19214506  8037

TINTIN B
1 43217U 18020C   18105.93439396 -.00000056 +00000-0 +60291-6 0  9995
2 43217 097.4630 114.1702 0016101 097.6203 262.6859 15.19282153007945
```

References

[1] K. Alfriend, S. Vadali, P. Gurfil, J. How, and L. Breger, *Spacecraft Formation Flying: Dynamics, Control, and Navigation*. Elsevier Astrodynamics Series, 2010.

[2] C. Stephen (2 April 2018). "Launch Log". Spaceflight Now. Archived from the original on 5 April 2018.

[3] C. Stephen (4 April 2018). "Dragon cargo capsule reaches space station for second time". Spaceflight Now. Retrieved 4 April 2018.

[4] Spaceflight101 (n.d.). Dragon - Cargo Version. Retrieved April 14, 2018, from http://spaceflight101.com/spacecraft/dragon/

[5] Spaceflight101 (n.d.). Dragon SpX-14 Cargo Overview. Retrieved April 23, 2018, from http://spaceflight101.com/dragon-spx14/cargo-overview/

[6] "Overview: SpaceX CRS-14 Mission" (PDF). NASA. Retrieved 4 April 2018.

[7] Grush, Loren (15 February 2018). "SpaceX is about to launch two of its space Internet satellites: the first of nearly 12,000". The Verge. Retrieved 16 February 2018.

[8] de Selding, Peter B. (2016-10-05). "SpaceX's Shotwell on Falcon 9 inquiry, discounts for reused rockets and Silicon Valley's test-and-fail ethos". SpaceNews. Retrieved 2016-10-08.

[9] Gates, Dominic (16 January 2015). "Elon Musk touts launch of 'SpaceX Seattle'". Seattle Times. Retrieved 19 January 2015.

[10] Messier, Doug (2017-03-03). "SpaceX Wants to Launch 12,000 Satellites". Parabolic Arc. Retrieved 2018-01-22.

[11] Musk, Elon (22 February 2018). "First two Starlink demo satellites, called Tintin A & B, deployed and communicating to Earth stations (video)". Twitter. Retrieved 22 February 2018.